

Single CdSe/CdS colloidal nanocrystals embedded in an Ultra-Pure SiO 2 matrix deposited by ion beam sputtering

Antoine Aubret, V Dolique, Agnès Piednoir, Christophe Dujardin, Florian Kulzer, Julien Houel

▶ **To cite this version:**

Antoine Aubret, V Dolique, Agnès Piednoir, Christophe Dujardin, Florian Kulzer, et al.. Single CdSe/CdS colloidal nanocrystals embedded in an Ultra-Pure SiO 2 matrix deposited by ion beam sputtering. Semiconductor Science and Technology, 2020, 35 (5), pp.055005. 10.1088/1361-6641/ab76fb . hal-03279125

HAL Id: hal-03279125
https://hal.science/hal-03279125

Submitted on 6 Jul 2021

HAL is a multi-disciplinary open access archive for the deposit and dissemination of scientific research documents, whether they are published or not. The documents may come from teaching and research institutions in France or abroad, or from public or private research centers.

L'archive ouverte pluridisciplinaire **HAL**, est destinée au dépôt et à la diffusion de documents scientifiques de niveau recherche, publiés ou non, émanant des établissements d'enseignement et de recherche français ou étrangers, des laboratoires publics ou privés.

Semiconductor Science and Technology

PAPER

Single CdSe/CdS colloidal nanocrystals embedded in an Ultra-Pure SiO_2 matrix deposited by ion beam sputtering

To cite this article: A Aubret *et al* 2020 *Semicond. Sci. Technol.* **35** 055005

View the article online for updates and enhancements.



IOP ebooks™

Bringing together innovative digital publishing with leading authors from the global scientific community.

Start exploring the collection–download the first chapter of every title for free.

This content was downloaded from IP address 137.110.35.63 on 12/04/2020 at 20:13

IOP Publishing Semiconductor Science and Technology
Semicond. Sci. Technol. 35 (2020) 055005 (7pp) https://doi.org/10.1088/1361-6641/ab76fb

Single CdSe/CdS colloidal nanocrystals embedded in an Ultra-Pure SiO_2 matrix deposited by ion beam sputtering

A Aubret[1,2], V Dolique[3], A Piednoir[1], C Dujardin[1], F Kulzer[1] and J Houel[1]

[1] Univ. Lyon, Université Claude Bernard Lyon 1, CNRS, Institut Lumière Matière, F-69622 Villeurbanne, France
[2] University of California San Diego (UCSD), Physics Department, 9500 Gilman Dr., La Jolla, CA 92093–0319, United States of America
[3] Laboratoire des Matériaux Avancés (LMA), IN2P3/CNRS, Université de Lyon, Lyon, France

E-mail: julien.houel@univ-lyon1.fr

Received 4 November 2019, revised 3 February 2020
Accepted for publication 17 February 2020
Published 25 March 2020

Abstract

We report the encapsulation of high-quantum-yield CdSe/CdS colloidal nanocrystals in a smooth and ultra-pure layer of SiO_2 deposited by ion beam sputtering. The optical quality of the thin silica film is comparable to the mirror substrates used in gravitational-wave detection, with a density of impurities as low as a few ppm. We show that at least 30% of the nanocrystals survive the encapsulation process under full conservation of their favorable optical properties at the single-quantum-dot level, namely a high and stable emission rate combined with a short recombination lifetime. The emission rate of the embedded nanocrystals is increased by 100% due to the higher refractive index of the SiO_2 film, in accordance with an effective-medium interpretation. Our device prototype thus provides a perspective for designing large-scale, high-quality and thickness-controlled light-emitting diodes based on semiconductor nanocrystals as active components in a durable inorganic matrix.

Keywords: quantum dots, CdSe/CdS, SiO_2, luminescence, nanocrystals, thin film

(Some figures may appear in colour only in the online journal)

1. Introduction

Quantum-dot-based light-emitting diodes (QD-LEDs) have attracted a lot of interest over the last 20 years [1]. These devices utilize the outstanding emission properties of colloidal QDs [2] at room temperature: close to 100% ON-state quantum yield (QY) [3], a wavelength that is easily tunable over the visible to near-IR range [1], high color-purity due to narrow emission linewidth [4], and industrial-scale synthesis. The first QD-LEDs were developed using organic materials as charge transport layers (CTLs) and QDs as active materials, starting at 0.01% quantum efficiency [5] and reaching up to 2.7% [6]. However, one critical issue of organic LEDs is the limited long-term stability of the CTLs [4] which requires an environmental packaging resistant to humidity and oxidation. All-inorganic QD-LEDs were therefore evaluated as a potential alternative, initially in form of n/p-GaN [7] as the CTLs, which was superseded by metal-oxides (ITO and NiO) [8], allowing to reach efficiencies of up to 0.1%. These relatively low efficiencies were attributed in part to the QDs being damaged by the deposition of the inorganic layers, leading to a reduction of the emission QY [4].

A recently proposed alternative design for all-inorganic QD-LEDs relies on high-frequency electroluminescence [9] of QDs that are embedded in an insulating matrix (Al_2O_3 or SiO_2); here, the QD luminescence is induced by high-frequency voltage sweeps that create electrons and holes at the QD/matrix interfaces, which in turn leads to photoluminescence (PL) from subsequent recombination processes. The main challenge in the fabrication of such insulator-based devices lies in conserving the favorable emission properties of the QDs in spite of the harsh environmental conditions employed by thin film deposition techniques suitable for insulators. Plasma-etching vapor deposition, for example,

 © 2020 IOP Publishing Ltd Printed in the UK

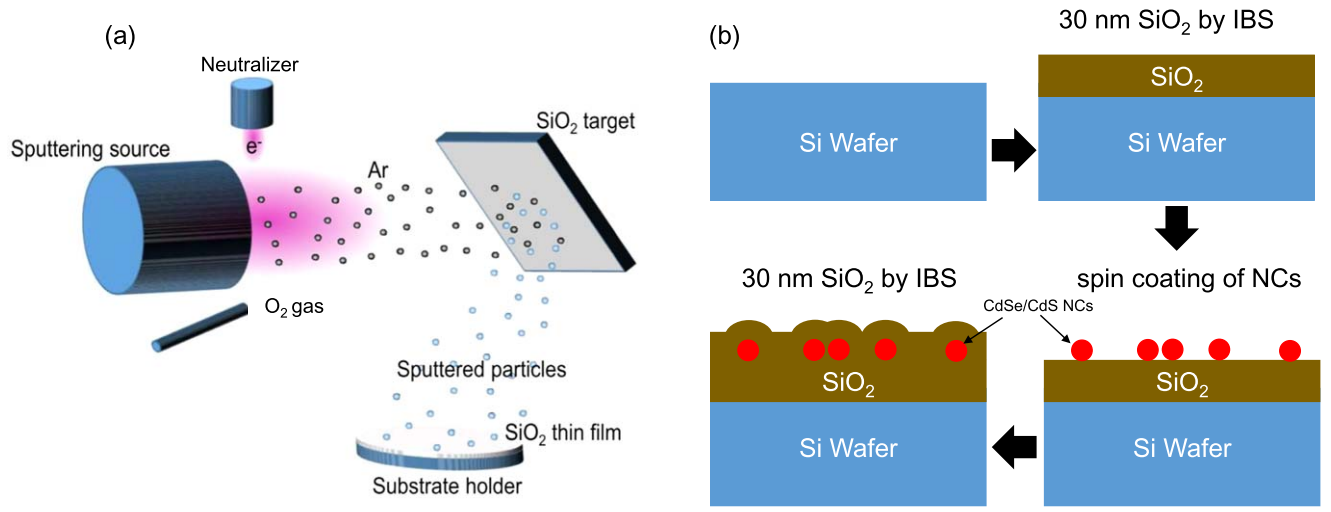


Figure 1. Fabrication of a device with CdSe/CdS nanocrystals (NCs) embedded in SiO_2. (a) Schematic illustration of layer deposition by IBS. (b) Three-step process of elaborating the SiO_2—QDs—SiO_2 sandwich structure.

uses a high-energy plasma and has already been shown to degrade the photoluminescence quantum yield of QDs in the resulting films [1]. Magnetron sputtering achieves better results in this respect [8–10], but has drawbacks in terms of controlling layer thickness precisely over large areas and ensuring an acceptably low density of defects. Ion beam sputtering (IBS) [11, 12] allows for a better control of deposition parameters such as target sputtering rate and the ion-current density; consequently, IBS combines high precision (0.7% fluctuation in coating thickness in an area of 500 mm diameter) with defect densities as low as a few ppm [13, 14]. This ultra-low defect density not only ensures high transparency even for thick layers, but also reduces the danger of mistaking matrix defects for single colloidal QDs [15, 16]. IBS being an established industry-scale technique, it seems ideally suited to produce high-quality QD-LEDs on a large-scale, featuring high deposition densities for ease of contacting and long-term device stability due to the protective function of inorganic films. In this work we show for the first time that high-quantum-yield colloidal QDs [17] can indeed be encapsulated in thin, ultra-pure SiO_2 films by IBS under conditions that allow to preserve the optical properties of a large fraction of the nanocrystals. Besides the implications for the fabrication of high-quality QD-LEDs discussed above, single QDs embedded in an insulating matrix are an interesting system for investigating many fundamental questions, for example the effect of high electric fields on QD optical emission (e.g. the quantum-confined Stark effect [18]).

2. Experimental section

CdSe/CdS colloidal QDs were synthesized following the protocol described in [17] and [19]. The resulting QDs had an overall diameter of 11 nm, with a CdSe core of diameter 4 nm surrounded by 3.5 nm thick CdS shell; their photoluminescence emission was centered at $\lambda = 600$ nm.

Three types of samples were used in the present work: First, a simple reference sample of free QDs was produced by spin-coating a 20 μl solution of CdSe/CdS QDs in hexane at 4000 rpm on a BK7 glass cover slip, resulting in a surface density of a few tens of QDs per 100 μm^2. Second, a pure SiO_2 film with a target thickness of 30 nm was deposited on a silicon wafer by IBS with a large-area ion beam deposition system (SPECTOR, Veeco Instruments Inc.), as schematically shown in figure 1(a). A voltage of 700 V with a current of 300 mA and an acceleration voltage of 150 V lead to a low-energy ion beam with a good stability of the plasma source. Finally, a device prototype consisting of a layer of QDs sandwiched between two layers of SiO_2 was fabricated in a three-step process on a silicon wafer as illustrated in figure 1(b): in the first step, a 30 nm layer of SiO_2 was deposited by IBS under the same conditions as detailed above. Next, a 40 μl solution of CdSe/CdS QDs in hexane was spin-coated at 4000 rpm on the SiO_2 layer to obtain a sheet density of hundred QDs per 25 μm^2. Finally, the QD layer was covered by a 30 nm layer of SiO_2 deposited by IBS with the same process parameters as for the first deposition. Special care was taken not to heat the substrate during the deposition processes (steps 1 and 3) in order to protect the wafer surface and the QDs.

The luminescence of single CdSe/CdS QDs was recorded with a home-built confocal microscope [20] that allowed for single-QD experiments with a spatial resolution of about 200 nm. The QDs were excited with a pulsed laser (Edinburgh Instruments, EPL-450) emitting at $\lambda = 445$ nm with a repetition rate between 5 and 20 MHz depending on the experiments. Emitted photons were detected with a single-photon-counting avalanche photodiode (Perkin Elmer, SPCM-AQ45) and lifetime histograms were compiled by a TimeHarp 200 card (Picoquant) operating in time-tagged time-resolved mode with an overall temporal resolution of the detection system of about 700 ps.

Atomic force microscopy (AFM) images were acquired with an MFP3D AFM (Asylum Research, Oxford Instruments)

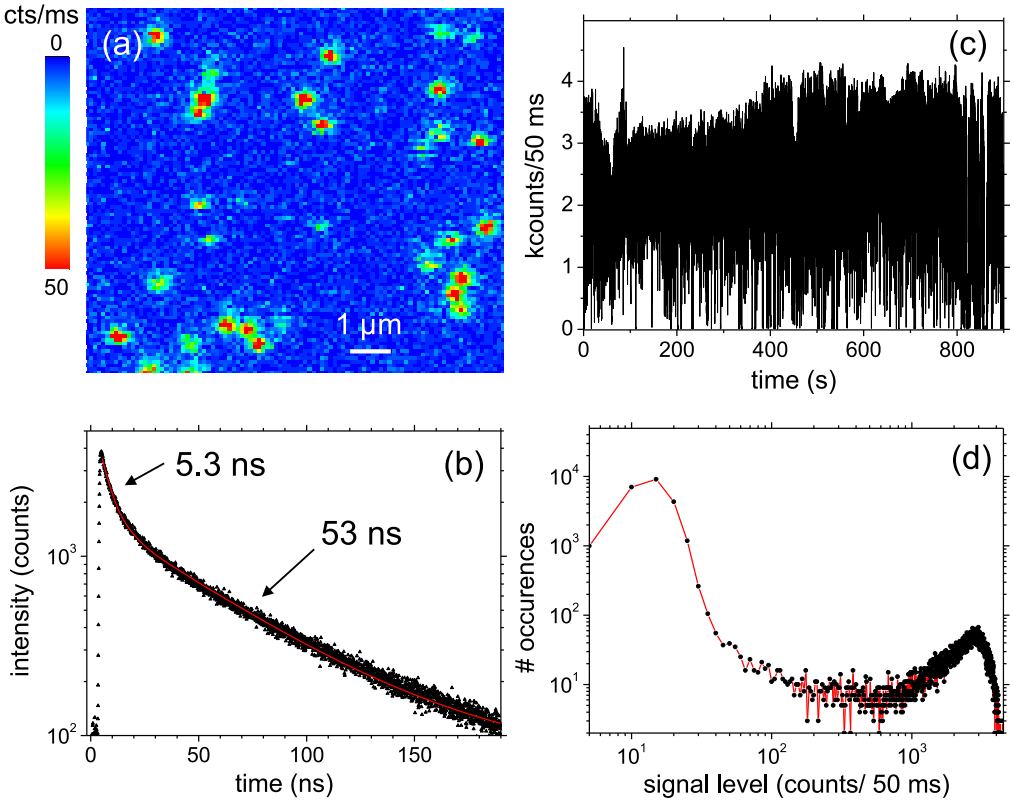


Figure 2. Photoluminescence properties of individual CdSe/CdS nanocrystals deposited on a BK7 coverslip (reference sample) (a) scanning confocal image of the photoluminescence intensity as a function of position. (b) Luminescence lifetime curve of a single CdSe/CdS QD. (c) The corresponding emission timetrace with a bin time of 50 ms recorded over 900 s. (d) Histogram of the number of counts observed in each 50 ms timebin of the timetrace (c).

operating in tapping mode with a silicon tip (Nanoworld ARROW-NCR, nominal spring constant 42 N m^{-1}, nominal tip radius 10 nm).

3. Results and discussion

The discussion of experimental results in this section is organized as follows: first we will document the luminescence properties of individual QDs in the reference sample, then we will characterize the topology of the pure SiO_2 layer, and finally we will present the photophysical properties of the QDs in the device prototype, comparing them to the reference sample to verify the non-destructiveness of the encapsulation process.

Figure 2(a) shows a 10 × 10 μm^2 confocal PL image of the reference sample, CdSe/CdS nanocrystals deposited on a BK7 glass substrate. The well-isolated spots represent the emission of individual QDs with detected count rates of up to 100 kHz. An example of an intensity timetrace of a single QD, i.e. its emission intensity as a function of time under prolonged excitation, is shown in figure 2(b); no photobleaching (irreversible loss of emission) occurred during the observation time of more than 850 s. The timetrace does exhibit the well-defined two-level blinking behavior that is characteristic for individual QDs alternating stochastically between two states of different emission intensity. These two states, which we will denote as 'bright' and 'dim', can be distinguished clearly in the histogram of the number of counts detected in 50 ms, figure 2(c), which shows two well-separated peaks at 11 counts (dim state) and at about 2500 counts (bright state), respectively. The existence of these two states furthermore manifests itself in the nanosecond-emission dynamics exemplified by the single-QD luminescence lifetime curve of figure 2(d), which was constructed from the histogram of observed delay times t between excitation pulses and photon detection events. This lifetime curve $I(t)$ is well fitted by a biexponential decay function on a non-zero background I_0

$$I(t) = I_0 + I_1\, e^{-t/\tau_{\mathrm{dim}}} + I_2\, e^{-t/\tau_{\mathrm{bright}}}. \qquad (1)$$

The two distinct exciton lifetimes are typical of two-level blinking of single CdSe/CdS-type nano-emitters [21], with the short lifetime corresponding to the dim state ($\tau_{\mathrm{dim}} = 5.3$ ns) and a long-time associated with the bright state ($\tau_{\mathrm{bright}} = 53$ ns). Note that in our case the dim state does not correspond to the dark $F = 2$ spin state [22], but rather to a charged state of the QD with a reduced luminescence quantum yield compared to the neutral exciton [23]. This reduced quantum yield and the shorter lifetime of the charged state are due to additional radiationless relaxation channels, which involve Auger processes and are therefore not accessible in the neutral state. As far the the bright state is concerned, we found $\langle\tau_{\mathrm{bright}}\rangle = (42.2 \pm 11.0)$ ns (average ± empirical standard deviation) for an ensemble of 10

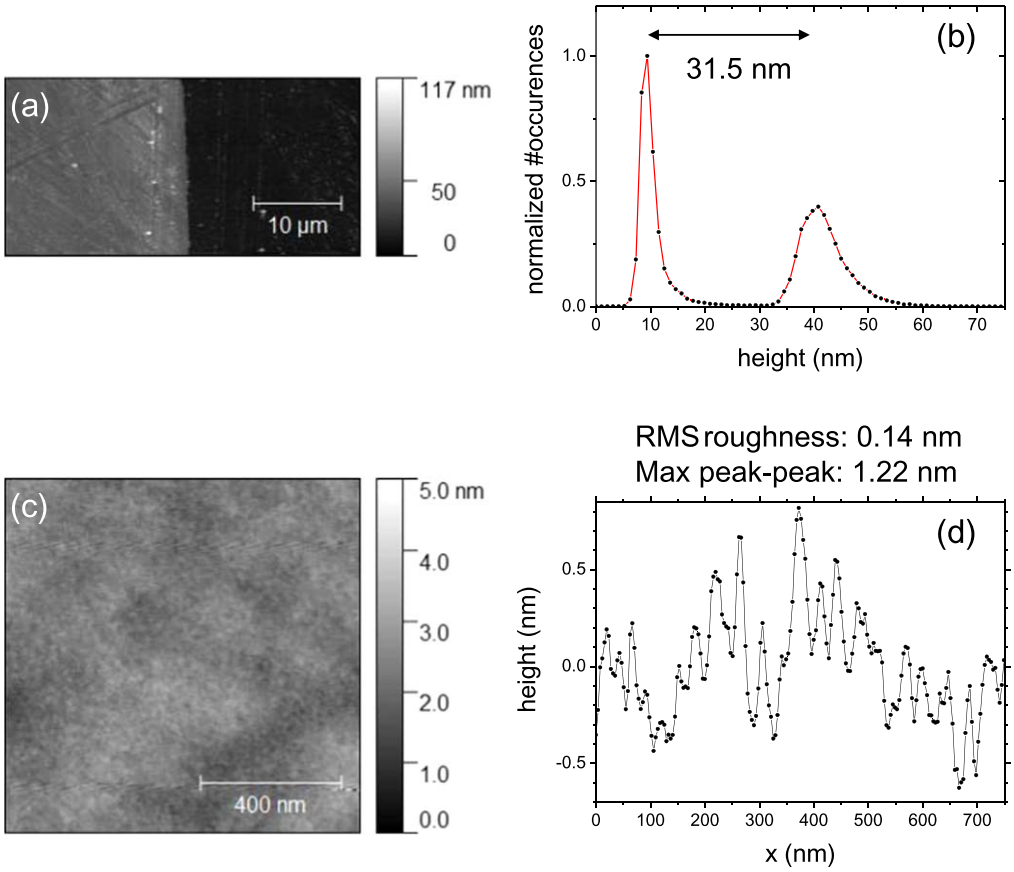


Figure 3. Surface quality of the deposited pure SiO_2 film. (a) AFM image of the transition from the bare silicon wafer to the SiO_2 layer. (b) Height histogram of a horizontal line profile measurement in image (a). (c) AFM image of a zoomed-in region of the SiO_2 layer. (d) Height along a line profile in (c) with RMS roughness and maximum peak-to-peak amplitude.

individual QDs on BK7. If the structural integrity of nanocrystals is compromised during the SiO_2 encapsulation process then one expects a reduction of both the overall emission intensity and the exciton lifetimes, as defects can entail long-lived dark states and additional radiationless recombination channels. It will therefore be important to compare the emission intensities and bright state lifetimes of the reference sample to the ones encountered for encapsulated QDs (see below).

Turning our attention to the deposition benchmark run, we present in figure 3(a) an AFM image of a region at the frontier between bare silicon and the deposited layer of pure SiO_2. This silicon-silica step was created by a stylus line that was left on the Si wafer during deposition and subsequently taken off by ethanol etching. The height histogram along a line drawn across the deposition boundary, figure 3(b), reveals a level difference of 31.5 nm between the surface of the silicon wafer and the top of the SiO_2 layer, meaning that the total thickness of the device prototype (with two identical SiO_2 deposition steps) is 63 nm. A local roughness measurement of an area of the SiO_2 layer far away for the step, figure 3(c), shows a flat surface over 1 μm^2 with a root-mean-square (RMS) roughness of 0.14 nm and a maximum peak-to-peak amplitude variation of 1.22 nm along the line profile of figure 3(d). The total RMS roughness calculated over the image of figure 3(c) is 0.04 nm. The small amplitude of these measured variations confirm the deposition of a high-quality, low-roughness layer of SiO_2.

The device prototype ($Si/SiO_2/QDs/SiO_2$ sandwich structure) was characterized by atomic force and confocal photoluminescence microscopy. Figure 4(a) shows an AFM image of a 25 μm^2 region of the device prototype, in which the top SiO_2 layer still exhibits a smooth surface, punctuated by small bumps (white dots) caused by the embedded single CdSe/CdS QDs. A spot-recognition algorithm [19] found 124 QDs in this image, indicated by the red circles in figure 4(b), which corresponds to a sheet density of (5.0 ± 0.4) QDs μm^{-2}. A zoomed-in measurement of a 1 μm^2 region of the same image is shown in figure 4(c), in which a few well-separated QDs appear as roughly Gaussian bumps of 9–11 nm height and a diameter of 25–35 nm at the base, see the line profiles of figures 4(d) and (e). The height of the bumps agrees very well with the diameter of 11 nm diameter that was deduced for these CdSe/CdS QDs in previous TEM measurements [19]. The lateral dimensions of the base are also compatible with the assumption of isolated individual QDs being observed, allowing for convolution effects arising from the non-zero radius of the AFM tip and a further potential enlargement due to the manner in which the SiO_2 matrix rearranges around each guest nanoparticle.

We present in figure 5(a) a confocal photoluminescence image of the device prototype. The intensity of the observed

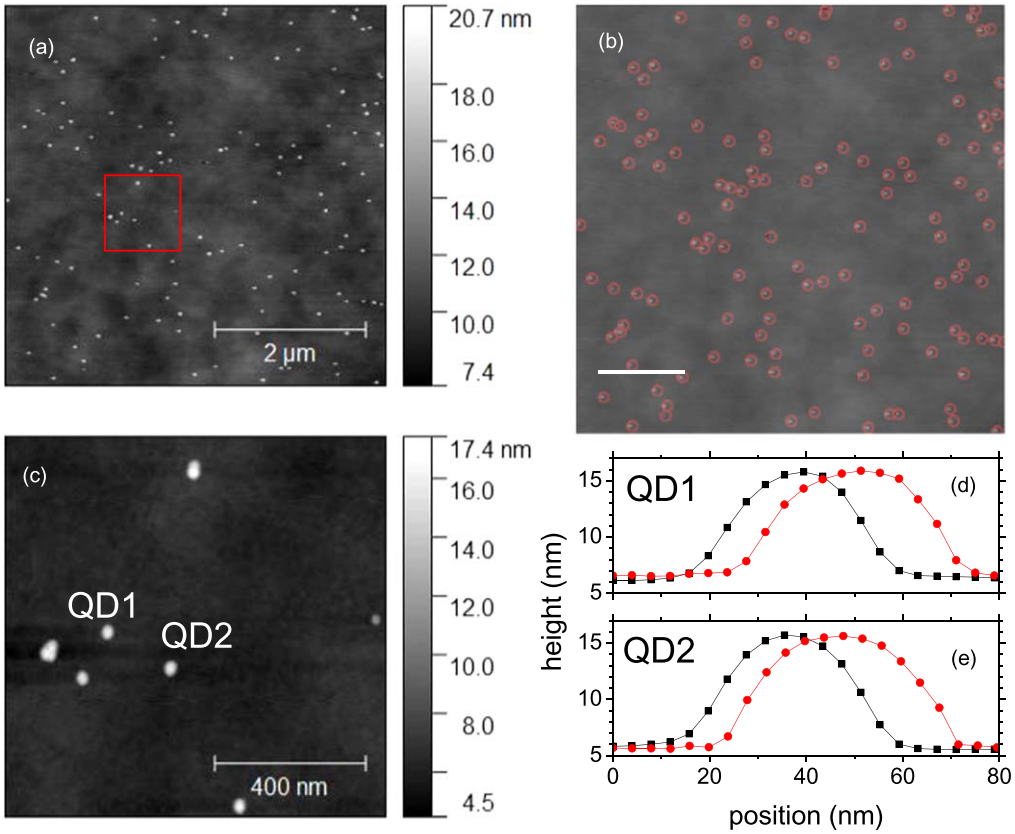


Figure 4. AFM characterization of the device prototype containing embedded CdSe/CdS nanocrystals.(a) 5 × 5 μm^2 region (256 × 256 pixels, pixel size 20 nm), in which raised bumps of individual QDs are visible as white dots. (b) Result of the spot-recognition algorithm applied to image (a); 124 QDs were identified and marked with red circled. The scale bar indicates 1 μm. (c) Zoomed-in AFM image of the 1 μm^2 area (256 × 256 pixels, 4 nm pixel size) indicated by the red rectangle in (a). (d), (e) Height profiles in the x and y directions through the centers of the spots labeled QD1 and QD2, respectively, in image (c).

single-QD spots was similar to the one obtained for the reference sample (bare QDs deposited on BK7, see figure 2), under comparable excitation conditions, which indicates that the luminescence quantum yield of the observed CdSe/CdS QDs was not significantly reduced by the encapsulation process. To estimate the surface density of luminescent QDs, we used the shape-recognition algorithm to count the number of photoluminescence spots in this image as illustrated in figure 5(b). We found a sheet density of (1.4 ± 0.1) QDs/μm^2, which amounts to about 30% of the density of QDs deduced from the AFM image of figure 4(a). This discrepancy may be due to a fraction of the QDs having been rendered non-luminescent during encapsulation, but it should be kept in mind that some of the luminescence spots may correspond to two or more QDs that are not resolved optically, but which would be counted as separate dots in an AFM image. (Our confocal microscope reached a resolution of about 200 nm, which is more than ten times lower than that of the AFM.) Furthermore, blinking processes (reversible temporary transitions to the dim state) can render a fraction of active QDs undetectable in any given scan image. We can therefore conclude that we have minimum survival rate of around 30% for the QDs during encapsulation, and that all the survivors seem to retain their remarkable luminescence properties.

Further evidence of the conserved luminescence quantum yield is given in figure 5(c), which presents a luminescence timetrace with maximum count rates of one million counts per second and clear two-level (bright/dim) blinking to confirm that an individual nano-emitter was observed [23]. The SiO_2 encapsulation process did not affect the long-time photostability either, as sustained emission of single QDs could be observed over a period of 900 s, see the example of figure 5(d) and compare to the reference sample, figure 2(c). Figure 5(e) shows a lifetime measurement of a single QD in device prototype, which was interpreted according to equation (1) to find the two lifetimes $\tau_{\mathrm{dim}} = 1.9$ ns and $\tau_{\mathrm{bright}} = 21$ ns, attributed to the dim and bright state, respectively. Measuring lifetimes of 10 QDs in the device prototype, we found $\langle \tau_{\mathrm{bright}} \rangle = (20.4 \pm 3.8)$ ns and $\langle \tau_{\mathrm{dim}} \rangle = (2.3 \pm 0.6)$ ns (average $\pm$ standard deviation). We thus observe that the bright state lifetime (neutral exciton) is reduced roughly by a factor of two compared to the reference sample of bare QDs on BK7 glass. To show that this reduced lifetime can be explained without invoking additional non-radiative relaxation channels, which could have been created due to degradation of the QD structure during the SiO_2 deposition process, we will estimate by how much the lifetime is expected to shorten simply because of the modification of the local refractive index as the emitters are embedded in

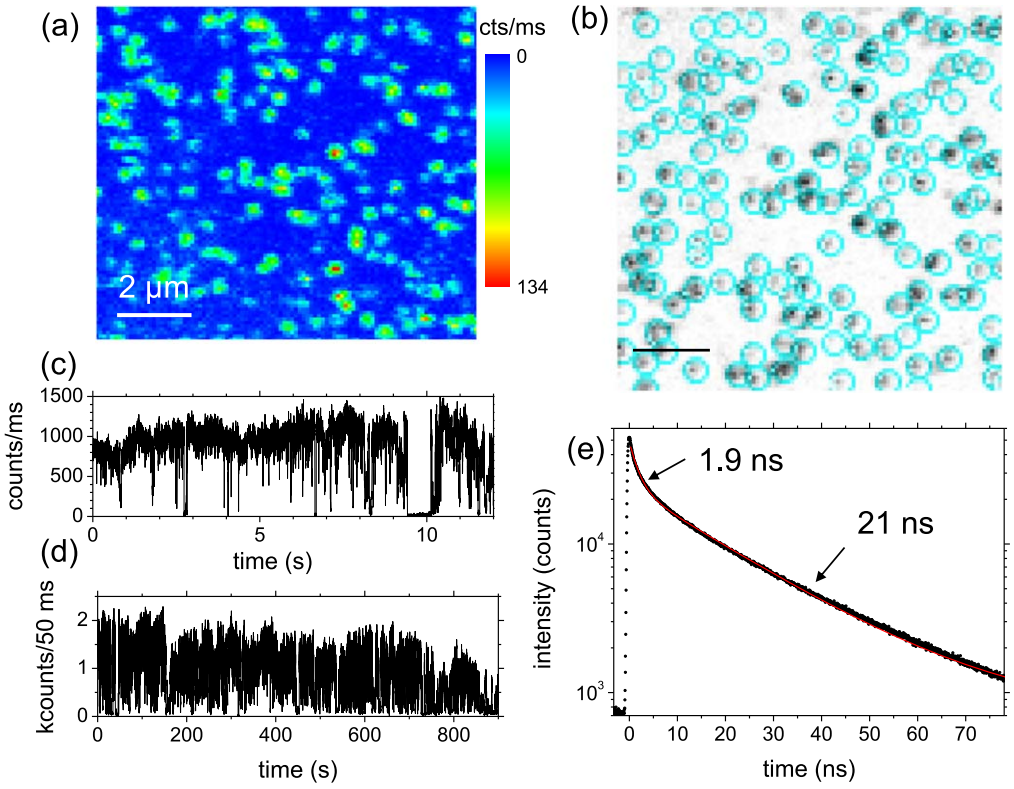


Figure 5. Photoluminescence properties of QDs in the device prototype. (a) $10 \times 10\ \mu m^2$ confocal luminescence image of single CdSe/CdS QDs embedded in the SiO_2 matrix. (b) Grayscale version of image (a), in which all QD spots identified by the shape-recognition algorithm have been marked with cyan circles. (c) Emission timetrace of an embedded single CdSe/CdS QD with saturated excitation. (d) Long-time intensity timetrace of a single CdSe/CdS QDs. (e) Photoluminescence lifetime curve of a single embedded CdSe/CdS nanocrystal fitted with a biexponential decay function, equation (1).

SiO_2. QD lifetimes are known to be sensitive to the refractive index of their local environment over distances varying from a few tens to few hundreds of nanometers [20, 24]. We use the virtual cavity (VC) model, which has been shown to fit the data for CdSe/ZnS QDs [20], to account for this phenomenon; the VC model can be summarized as

$$\gamma_{\mathrm{vac}} = \frac{\gamma_{\mathrm{ref}}}{\bar{n}_{\mathrm{ref}}}\left(\frac{3}{\bar{n}_{\mathrm{ref}}^2 + 2}\right)^2 \quad \text{and} \tag{2}$$

$$\gamma_{\mathrm{mat}} = \left(\frac{\bar{n}_{\mathrm{mat}}^2 + 2}{3}\right)^2 \bar{n}_{\mathrm{mat}}\, \gamma_{\mathrm{vac}}, \tag{3}$$

where γ_{ref}, γ_{mat} and γ_{vac} are the neutral exciton recombination rates of a QD on a BK7 coverslip, in the SiO_2 matrix and in vacuum, respectively, while $\bar{n}_{\mathrm{ref}}$ and $\bar{n}_{\mathrm{mat}}$ are the *effective* refractive indices experienced by QDs on BK7 (reference sample) and in the SiO_2 matrix (device prototype). We calculated these effective refractive indices as described previously [20], using a hard-sphere model with a radius of 50 nm and a core-centered emission dipole in the framework of the Bruggeman effective medium approach [25]. For the reference sample ($n_{\mathrm{BK7}} = 1.52$ at 600 nm) we find $\bar{n}_{\mathrm{ref}} = 1.21$, while the effective refractive index for the device prototype ($n_{\mathrm{Si}} = 3.95$, $n_{\mathrm{SiO_2}} = 1.46$) is $\bar{n}_{\mathrm{mat}} = 1.46$. Inserting $\bar{n}_{\mathrm{ref}}$ and $\gamma_{\mathrm{ref}} = 0.024\ \mathrm{ns}^{-1}$ (from the measured $\tau_{\mathrm{bright}} = 42.2$ ns) into the VC model of equation (2), we obtain $\gamma_{\mathrm{vac}} = 0.015\ \mathrm{ns}^{-1}$, which corresponds to an exciton recombination lifetime in vacuum of $\tau_{\mathrm{vac}} = 67$ ns. The value of γ_{vac} thus identified leads to an expected radiative lifetime for the device prototype of $\tau_{\mathrm{bright}} = 24.4$ when used in equation (3) with the value of $\bar{n}_{\mathrm{mat}}$ given above. We can thus conclude that the observed lifetime of $\tau_{\mathrm{bright}} = 20.4$ in the device prototype agrees very well with the expected effect of the increased local refractive index. In combination with the remarkably high detected count rates documented above, this observation further supports the hypothesis that the IBS encapsulation process manages to preserve the structural integrity of the nanocrystals and does not entail the creation of additional non-radiative relaxation channels.

4. Conclusion

We have documented the first successful encapsulation of colloidal CdSe/CdS QDs in a thin film of SiO_2 deposited by IBS. Our protocol yielded a smooth and ultra-pure matrix, in which we could detect the luminescence of individual QDs with count rates of up to one MHz that were sustained without photobleaching during observation times of several hundreds of seconds. These remarkable count rates and the excellent photostability indicate that the favorable photophysical properties of free QDs on BK7 glass have been fully conserved. A combination of optical confocal and AFM furthermore allowed us to establish an encapsulation survival

rate at the single-QD level of at least 30%. An observed reduction of the exciton lifetime by a factor of two after encapsulation was shown to be consistent with the expected influence of the increased local refractive index in the QD-in-SiO_2 device prototype, which further supports the conclusion that the active nano-emitters have not suffered any significant structural degradation. Our results thus establish a potential technique for fabricating SiO_2-based, ultra-pure field-effect devices with quantum dots as active emitters based on an industry-scale process. In the future one may even hope to extend the technique to other nanoemitters such as perovskites and more environment-friendly graphene-based species.

ORCID iDs

J Houel https://orcid.org/0000-0003-3901-0882

References

[1] Shirasaki Y, Supran G J, Bawendi M G and Bulović V 2013 *Nat. Photon.* **7** 13–23
[2] Murray C B, Norris D J and Bawendi M G 1993 *J. Am. Chem. Soc.* **115** 8706–15
[3] Jeong B G *et al* 2016 *ACS Nano* **10** 9297–305
[4] Wood V and Bulović V 2010 *Nano Rev.* **1** 5202
[5] Colvin V L, Schlamp M C and Alivisatos A P 1994 *Nature* **370** 354–7
[6] Anikeeva P O, Halpert J E, Bawendi M G and Bulović V 2007 *Nano Lett.* **7** 2196–200
[7] Mueller A H, Petruska M A, Achermann M, Werder D J, Akhadov E A, Koleske D D, Hoffbauer M A and Klimov V I 2005 *Nano Lett.* **5** 1039–44
[8] Caruge J M, Halpert J E, Wood V, Bulović V and Bawendi M G 2008 *Nat. Photon.* **2** 247–50
[9] Bozyigit D, Wood V, Shirasaki Y and Bulović V 2012 *J. Appl. Phys.* **111** 113701
[10] Levichev S, Chahboun A, Basa P, Rolo A G, Barradas N P, Alves E, Horvath Z J, Conde O and Gomes M J M 2008 *Microelectron. Eng.* **85** 2374–7
[11] Honig R E 1958 *J. Appl. Phys.* **29** 549–55
[12] Sassolas B, Flaminio R, Franc J, Michel C, Montorio J L, Morgado N and Pinard L 2009 *Appl. Opt.* **48** 3760–5
[13] Beauville F *et al* 2004 *Proc. SPIE* **5250** 483–92
[14] Pinard L *et al* 2017 *Appl. Opt.* **56** C11–C15
[15] Wang X Y, Ren X F, Kahen K, Hahn M A, Rajeswaran M, Maccagnano-Zacher S, Silcox J, Cragg G E, Efros A L and Krauss T D 2015 *Nature* **527** 544
[16] Rabouw F T, Cogan N M B, Berends A C, van der Stam W, Vanmaekelbergh D, Koenderink A F, Krauss T D and Donegá C D 2016 *Sci. Rep.* **6** 21187
[17] Mahler B, Spinicelli P, Buil S, Quélin X, Hermier J P and Dubertret B 2008 *Nat. Mater.* **7** 659–64
[18] Empedocles S A and Bawendi M G 1997 *Science* **278** 2114–7
[19] Houel J *et al* 2015 *ACS Nano* **9** 886–93
[20] Aubret A, Pillonnet A, Houel J, Dujardin C and Kulzer F 2016 *Nanoscale* **8** 2317–25
[21] Galland C, Ghosh Y, Steinbrück A, Hollingsworth J A, Htoon H and Klimov V I 2012 *Nat. Commun.* **3** 908
[22] Efros A L, Rosen M, Kuno M, Nirmal M, Norris D J and Bawendi M 1996 *Phys. Rev.* B **54** 4843–56
[23] Nirmal M, Dabbousi B O, Bawendi M G, Macklin J J, Trautman J K, Harris T D and Brus L E 1996 *Nature* **383** 802–4
[24] LeBihan V, Pillonnet A, Amans D, Ledoux G, Marty O and Dujardin C 2008 *Phys. Rev.* B **78** 113405
[25] Aspnes D E 1982 *Am. J. Phys.* **50** 704–9